EFFECT OF LOW-SPEED IMPACT DAMAGE AND DAMAGE LOCATION ON BEHAVIOR OF COMPOSITE PANELS

Dawn Jegley

NASA Langley Research Center
Hampton, Virginia

ABSTRACT

An investigation of the effects of low-speed impact damage on the compression and tension strength of thin (less than .05 inches thick) and moderately thick (between .12 and .17 inches thick) composite specimens was conducted. Impact speeds ranged from 50 to 550 ft/sec (impact energies from .25 to 30.7 ft-lb) and impact locations were near or away from a lateral unloaded edge. In this study, thin tension-loaded or compression-loaded specimens with only 90° and ±45° plies which were impacted away from the unloaded edge suffered less reduction in maximum load-carrying capability due to impact damage than the same specimens impacted near the unloaded edge. Unlike the thin laminates, failure loads of thicker compression-loaded specimens with a similar stacking sequence were independent of impact location. Failure loads of thin tension-loaded specimens with 0° plies were independent of impact location while failure loads of thicker compression-loaded specimens with 0° plies were dependent upon impact location. A finite-element analysis of strain distributions across the panel width indicated that high axial strains occur near the unloaded edges of postbuckled panels, indicating that impacts near the unloaded edge would significantly effect the behavior of postbuckled panels.

INTRODUCTION

For composite parts to be used on aircraft primary structure, the effects of low-speed impact damage on the behavior of these structures must be understood. Impact damage followed by compression or tension loading is an important condition to be considered in the design of aircraft with composite structures. Both thicker laminates for wing panels and thinner laminates for fuselage skins must be studied. A great deal of work has been done on the effects of impact damage in the center of a relatively thick specimen (e.g., references 1-3) loaded in compression. This type of impact damage is representative of impact damage in a wing panel away from a supported edge or a stiffener. Less work has been done on impact damage near a support location or a stiffener on thinner specimens. However, impact damage near a stiffener or a supported edge can be a critical problem in compression-loaded structures (see reference 4) and damage tolerance criteria for thick specimens, such as allowable indentation depth, are not always applicable to thin specimens. Although fuselage structures carry tensile as well as compressive loads, the effect of impact location on tension-loaded panels is largely unexplored. Some data on tension-loaded specimens impacted away from a support are presented in references 5 and 6, but more work needs to be done to quantify the effects of panel thickness and impact location on structural performance.

The objective of this paper is to discuss the effects of impact damage location on failure of thin and moderately thick composite structures and to provide an

explanation for this behavior. The results of an investigation of the behavior of graphite-epoxy and graphite-thermoplastic specimens subjected to low-speed impact damage at the center of the specimen and near an unloaded edge are presented in the present paper. Tension-loaded specimens, whose behavior is dependent upon material characteristics, are discussed first. Compression-loaded specimens, whose behavior is dependent upon both material characteristics and structural parameters, are then discussed.

TEST SPECIMENS

The graphite-epoxy specimens tested in this investigation were fabricated from commercially available Hercules, Inc., AS4[+] graphite fiber and 3502[+] thermosetting epoxy resin. The graphite-thermoplastic specimens were fabricated from commercially available Hercules AS4 graphite fiber and ICI PEEK[+] thermoplastic resin. All graphite-epoxy and some graphite-thermoplastic specimens were fabricated from unidirectional tape. The remaining graphite-thermoplastic specimens were fabricated from woven fabric in which the +45° and -45° fibers were woven together. The specimens tested in this study were made from the four stacking sequences $[(\pm 45)_2/\overline{90}]_s$, $[(\pm 45)_2/90]_{3s}$, $[\pm 45/0_2]_s$ and $[\pm 45/0_2]_{3s}$, which include a range of thicknesses. Specimen dimensions are shown in table I. All specimens were nominally 10 or 14 inches long and either 3, 4, or 10 inches wide with width-to-thickness ratios ranging from 18 to 240. All specimens were ultrasonically C-scanned to establish specimen quality prior to testing. Tabs were bonded to the tension-loaded specimens to prevent damage from being induced by the grips of the testing machine. The configuration of a typical tension specimen is shown in figure 1(a). The loaded ends of each compression specimen were machined flat and parallel to permit uniform end displacement.

APPARATUS AND TESTS

Tension Tests

Test specimens were slowly loaded in tension in an MTS testing machine using hydraulic grips. The unloaded edges were unsupported during the test. The applied load and change in specimen length were recorded at regular intervals during the test.

Compression tests

Test specimens were slowly loaded in uniaxial compression using a hydraulic testing machine. The loaded ends of the specimen were clamped by fixtures during testing, and the unloaded lateral edges were simply supported by knife-edge restraints to prevent the specimen from buckling as a wide column. A typical compression specimen mounted in the support fixture is shown in figure 1(b). Electrical resistance strain gages were used to monitor strains, and dc differential transformers were used to monitor displacements. Typical locations of back-to-back strain gages used to monitor far-field laminate strains are shown in figure 1(b).

[+]Identification of commercial products and companies in this paper is used to describe adequately the materials. The identification of these commercial products does not constitute endorsement, expressed or implied, of such products by the National Aeronautics and Space Administration.

All specimens loaded in compression were painted white on one side to provide a reflective surface so that a moire fringe technique could be used to monitor out-of-plane deformation patterns. The applied load, the displacement of the loading platen, and the strain gage signals were recorded at regular intervals during the test.

Impact Damage

A procedure described in reference 7 was used in the current study for impacting specimens. Aluminum spheres 0.5 inches in diameter were used as impact projectiles. The projectiles were directed normal to the plane of the specimen at speeds from 50 to 550 ft/sec. One specimen of each type was not impacted and used as a reference or control specimen while the remaining specimens were impacted prior to loading. All impacted specimens were impacted at midlength and either at midwidth or near a lateral unloaded edge. Compression-loaded specimens were placed in the test fixture prior to impact. Lateral locations of impact sites are indicated in figure 1. Since impact speed alone does not fully describe an impact event, the range of impact speeds considered and the corresponding impact energy is shown in table II.

ANALYTICAL MODEL

Finite-element models of the graphite-epoxy compression-loaded control specimens were developed. A uniform grid of quadrilateral plate elements was used. The number of elements used to model each specimen was dependent upon the specimen dimensions but in each case the elements used were approximately square. At least 30 elements were used in the axial direction for each model. To simulate clamped conditions, no displacements or rotations were permitted on one end of the specimen and only the axial displacement was permitted on the opposite (loaded) end. The axial displacement was forced to be constant along the loaded edge. To simulate the simply supported edges, no out-of-plane displacements along the unloaded lateral edges were permitted. All analytical results are based on material properties given in table III and a nonlinear analysis using the finite-element computer code STAGS (reference 8).

RESULTS AND DISCUSSION

Test results for specimens constructed with the four stacking sequences listed in table I are presented in this section. A comparison is made between specimens with the same stacking sequence impacted with the same impact energy in the center of the test section and impacted near a lateral unloaded edge (free for tension specimens, simply supported for compression specimens). Experimentally determined failure loads and strains are discussed for tension-loaded specimens; and then experimentally determined failure loads, buckling loads, strain distributions and out-of-plane deformations are discussed for compression-loaded specimens. Finite-element predictions of displacements and strains and experimental results are presented for specimens loaded into the postbuckling range. Results are presented in terms of a "normalized load" (load divided by specimen cross-sectional area) and "normalized end-shortening" (end-shortening divided by specimen length), and are not referred to as an "average stress" and "average strain." The terms "average stress" and "average strain" could be misleading since stresses and strains in the specimen after buckling are not constant across the width of the panel.

Tension-loaded Specimens

Graphite-epoxy specimens constructed with two different stacking sequences were loaded in tension. One control specimen (a specimen without impact damage) of each stacking sequence was tested. Half the remaining specimens were impacted midlength and midwidth (x/b =.5, where x is the distance from the specimen unloaded edge to the impact site and b is the specimen width) and half were impacted .75 inches from an unloaded edge (x/b=.25). All specimens were loaded to failure and showed extensive damage due to failure. Control specimens failed near the tabs while impact damaged specimens failed through the impact site. The normalized failure load (applied load at failure P divided by initial cross-sectional area A) of the control specimens is shown in table I. The nominal impact speeds, impact locations and normalized failure loads are shown in table IV for all impacted tension-loaded specimens.

The effect of impact damage on the maximum load-carrying capability of these specimens is presented in figure 2 which shows the relationship between normalized failure load and impact speed. The circular symbols in the figure represent failures of specimens impacted near an unloaded edge and the square symbols represent failure of specimens impacted in the center of the specimen. Impacts which caused no visible damage are represented by open symbols. Impacts which caused visible damage are represented by shaded symbols if the impactor did not pass through the specimen and by filled symbols if the impactor did pass through the specimen.

The maximum reduction in load-carrying capability demonstrated in the centrally impacted specimens is 32 and 25 percent of the load-carrying capability of the corresponding undamaged (control) specimens for the $[(\pm 45)_2/\overline{90}]_s$ and $[\pm 45/0_2]_s$ specimens, respectively. In each case, the maximum reduction for the centrally impacted specimen occurs for impact speeds of 300 ft/sec. The maximum reduction for side-impacted specimens is 49 and 30 percent of the load-carrying capability of the control specimens for the $[(\pm 45)_2/\overline{90}]_s$ and $[\pm 45/0_2]_s$ specimens, respectively. For the $[(\pm 45)_2/\overline{90}]_s$ specimens, the centrally impacted specimens carry slightly more load at failure than the side-impacted specimens for all impact speeds considered. However, the side-impacted $[\pm 45/0_2]_s$ specimen impacted at 400 ft/sec has a higher failure load than the centrally impacted specimen impacted at the same speed. This result suggests that impact location has no influence on maximum load-carrying capability for $[\pm 45/0_2]_s$ specimens when loaded in tension. The 400 ft/sec impacts cause less reduction in load-carrying capability than the 300 ft/sec impacts for the $[\pm 45/0_2]_s$ specimens. This same behavior is described for $[0/90]_{3s}$ specimens in reference 6.

In the study described in reference 6, the most damage was caused when the impact speed was just sufficient to cause the impactor to pass through the specimen. Different types of damage are caused by impacts at different speeds. Low-speed impacts cause delaminations within the specimen. Higher-speed impacts for which the impactor does not pass through the specimen, and impacts for which the impactor barely passes through the specimen cause delaminations and severe damage to the back of the specimen, including fiber breakage. Very high speed impacts, for which the impactor passes through the specimen, cause very high stress at the impact site and less cracking away from the impact site. These different types of damage can lead to different failure modes and different amounts of reduction in maximum load-carrying capability.

Compression-loaded Specimens

Control Specimens

Control specimens (those without impact damage) for each stacking sequence were loaded in compression. Six control specimens with stacking sequence $[(\pm 45)_2/\overline{90}]_s$ were loaded to failure. A three-inch-wide specimen and a four-inch-wide specimen were each constructed from graphite-epoxy tape, graphite-thermoplastic tape and graphite-thermoplastic fabric. The three-inch-wide specimens buckled into one transverse and four axial half-waves of nearly equal wavelength then failed at specimen midlength (along a nodal line). The four-inch-wide specimens buckled into one transverse and three axial half-waves then failed at a nodal line. Each specimen carried load well into the postbuckling range. Normalized failure loads are shown in table I.

Two moderately thick control specimens with stacking sequence $[(\pm 45)_2/90]_{3s}$ were constructed from graphite-epoxy tape and loaded to failure. One specimen was three inches wide and one was four inches wide. Both specimens buckled into one transverse and three axial half-waves immediately prior to failure. The three-inch-wide specimen failed through the center of the specimen (not a nodal line). The four-inch-wide specimen failed at a nodal line. Normalized failure loads are shown in table I.

One thin control specimen with stacking sequence $[\pm 45/0_2]_s$ and one moderately thick control specimen with stacking sequence $[\pm 45/0_2]_{3s}$ were made from graphite-epoxy tape and tested. Each specimen was 10 inches wide and 14 inches long. These control specimens buckled into one half-wave in each direction prior to failure near a loaded edge. The normalized failure load of the $[\pm 45/0_2]_{3s}$ control specimen is shown in table I. The $[\pm 45/0_2]_s$ control specimen was not loaded to failure.

Impact Damaged Specimens

All remaining compression-loaded specimens were subjected to impact damage prior to loading. Nominal impact speeds, impact locations and normalized failure loads are shown in tables V-VII for the compression-loaded specimens with 3-, 4- and 10-inch widths, respectively.

$[(\pm 45)_2/\overline{90}]_s$ Specimens.- The relationship between impact speed and normalized failure load is shown in figures 3(a), 3(b) and 3(c) for specimens fabricated from graphite-epoxy tape, graphite-thermoplastic tape and graphite-thermoplastic fabric, respectively. The circular symbols in each figure represent the failure of the side-impacted specimens and the square symbols represent the failure of centrally impacted specimens. Impacts which caused no visible damage are represented by open symbols. Impacts which caused visible damage are represented by shaded symbols if the impactor did not pass through the specimen and by filled symbols if the impactor passed through the specimen. Specimens subjected to impact speeds less than about 200 ft/sec buckled into 4 axial half-waves and then failed at the nodal line through the impact site. Specimens subjected to impact at higher impact speeds buckled into 3, 4 or 5 axial half-waves along the length and failed through the impact site whether or not the impact site was located on a nodal line. Each specimen failed by transverse cracking and many also exhibited off-axis cracking and fiber separation on the side opposite the impact site.

Impacts at 100 ft/sec caused no reduction in maximum load-carrying capability. The results show a significant reduction in normalized failure load for each type of specimen as impact speed increases from 100 to 300 ft/sec. For the graphite-epoxy specimens, a centrally located impact can reduce the maximum load-carrying

capability of a specimen by up to 12 percent compared to that of an undamaged specimen. However, for the graphite-thermoplastic specimens, a centrally located impact can reduce the maximum load-carrying capability by 30-35 percent. The impact speed causing the most reduction in maximum load-carrying capability of the graphite-epoxy specimen is 225 ft/sec while the impact causing the most reduction in maximum load-carrying capability of the graphite-thermoplastic specimen is 300 ft/sec.

The results shown in figure 3 indicate a dependence of normalized failure load on impact location. An impact .75 inches from the lateral unloaded edge of a 3-inch-wide specimen causes a reduction in maximum load-carrying capability of about 35 percent for each type of specimen; i.e., three times the reduction in the graphite-epoxy centrally impacted specimens but about the same as the reduction in the graphite-thermoplastic centrally impacted specimens. The effect of impact location on maximum load-carrying capability is more significant for graphite-epoxy specimens than for graphite-thermoplastic specimens; however, the trend is the same for both materials. A side impact reduces the maximum load-carrying capability of the specimen by at least as much as a central impact for a given impact speed.

For these three types of specimens, nonvisible damage did not reduce their maximum load-carrying capability and the impact speed producing barely visible damage was approximately 170 ft/sec. Impacts causing visible damage caused extensive reduction in maximum load-carrying capability. In general, the most severe reduction occurred when the impact speed was approximately the speed necessary to cause the impactor to pass through the specimen. This speed was approximately 240, 325, and 275 ft/sec for the graphite-epoxy tape, the graphite-thermoplastic tape and the graphite-thermoplastic fabric specimens, respectively. An impactor that passed through the specimen at high speed (e.g., 500 ft/sec) caused less damage than an impactor that bounced off the specimen. This difference in the amount of damage is the reason that a damaged specimen with a through penetration has a higher maximum load-carrying capability than a damaged specimen without a through penetration. Ultrasonic C-scans of specimens after impact and before compressive loading indicate that there is a significant decrease in damage area for very high speed impacts compared to impacts in which the impactor barely passes through the specimen for the graphite-thermoplastic specimens. A small decrease in damage area is seen for very high speed impacts for the graphite-epoxy specimens. However, the failure load does not always correlate with the damage area determined by C-scan, as demonstrated in reference 3 for several stacking sequences. This lack of correlation is attributed to the fact that C-scan indicates a total damage area in a qualitative manner, not a specific amount and type of damage (i.e., number and location of delaminations) in the area.

The relationship between normalized failure load and impact location is shown in figure 4 for a four-inch-wide specimen impacted at several locations across the width at a speed of approximately 450 ft/sec (the impactor passed through the specimens). In each case the central impact caused little reduction in maximum load-carrying capability but the side impacts caused a significant reduction. The closer the impact was to the edge of the specimen, the more the reduction in maximum load-carrying capability. A discussion of why a side impact causes more reduction in maximum load-carrying capability than a center impact is presented later in this paper.

The experimentally determined normalized load versus normalized end-shortening of four impacted graphite-epoxy specimens is shown in figure 5. The load is normalized by the specimen cross-sectional area and the end-shortening is normalized

by the specimen length. Two specimens were impacted at 175 ft/sec (damage which was barely visible) and two specimens were impacted at 250 ft/sec (the impactor passed through the specimen). Each specimen buckled at a normalized load of approximately 10 ksi. There is no difference between the prebuckling response of the side- and center-impacted specimen in either case. The primary difference in the postbuckling response is that the side-impacted specimens fail at much lower loads than the center-impacted specimens.

The displacements and strains in the four-inch-wide control specimen are shown in figure 6. The experimentally determined normalized load versus normalized end-shortening relationship for three four-inch-wide specimens and the analytically determined normalized load versus normalized end-shortening relationship for a four-inch-wide control specimen are shown in figure 6(a). The analytical and experimental results for the control specimen agree quite well. The control specimen fails at a load 2.61 times the buckling load. Little difference is seen between the results for the centrally impacted specimen and the control specimen but the side-impacted specimen failed at a much lower load, although the overall specimen stiffness seems to be unaffected by the impact damage.

The analytically determined out-of-plane displacements w (normalized by the specimen thickness t) along the specimen length L at the center, at one quarter of the width and near an unloaded edge, for a specimen loaded in the postbuckling range is shown in figure 6(b). The buckling load of the specimen is represented by P_{cr} and the specimen buckled into one transverse and three axial half-waves. Displacements for 1.22 and 2.55 times the buckling load are shown. The maximum out-of-plane displacement is at the center of the specimen. The highest gradient in out-of-plane deformation is at the nodal lines, at approximately y/L= .33 and .66 (y is distance from the loaded edge).

The experimentally determined axial membrane strain (average of back-to-back strain gages) across the specimen at a nodal line is shown in figure 6(c) for several values of load P, normalized by the buckling load P_{cr}, in the pre- and postbuckling range. In the postbuckling range, the higher the value of P/P_{cr}, the higher the membrane strain near the unloaded edge of the specimen and the lower the membrane strain near the center of the specimen. The strain distribution across the specimen width at a nodal line just before failure is shown in figure 6(d). The dashed and solid curves represent membrane strains determined analytically and experimentally, respectively (a least squares fit to the data points was used). The open and filled symbols represent surface strains determined analytically and experimentally, respectively. Slight differences in results at the unloaded edges can be attributed to anisotropic effects since the ratios of the anisotropic terms to the bending stiffnesses are relatively large, i.e., D_{16}/D_{11}=.22, and D_{26}/D_{22}=.31. Front and back surface strains differ significantly in the postbuckled specimen, and much higher strains occur at the edges of the specimen than at the center.

The strain and displacement distributions presented in figure 6 indicate why side impacts have more effect on failure loads than central impacts for these buckled specimens. Prior to buckling, the axial strain is relatively constant across the width of the panel so impact location has little effect on specimen behavior. At buckling, the loads in the panel redistribute and more load is carried near the supported unloaded edges. The high deformation gradients at the nodal lines and the higher strains near the specimen edges induce transverse shearing loads which cause failure at the nodal lines in undamaged specimens. Impact damage in a region of high strain near an unloaded edge has more effect on strength than impact damage in a region of low strain at the specimen center.

$[(\pm 45)_2/90]_{3s}$ Specimens.- A series of moderately thick three-inch-wide specimens were impacted either in the center of the specimen or .7 inches away from an unloaded edge. The relationship between normalized failure load and impact speed is shown in figure 7 for these specimens. The specimen impacted midwidth at 100 ft/sec buckled into three axial half-waves immediately prior to failure. No other impacted specimen buckled. The most severe reduction in maximum load-carrying capability due to impact damage occurs at a speed of 400 ft/sec, but there appears to be no difference between the effect of side impact and center impact. The impactor passed through the specimen at speeds greater than about 425 ft/sec and the failure load increased slightly for speeds of 525 ft/sec since a more ballistic type of damage is induced at very high speeds (ref. 6). Nonvisible damage does not cause a reduction in maximum load-carrying capability, but barely visible damage (impact speeds of 150 ft/sec) causes more than a 40 percent reduction in maximum load-carrying capability compared to the control specimen.

The relationship between normalized failure load and impact location for four four-inch-wide specimens impacted at a speed of 500 ft/sec is shown in figure 8. Impact location appears to have little effect on failure load. The normalized load versus normalized end-shortening for three specimens impacted at 540 ft/sec is shown in figure 9. The control specimen buckles just before failure while the impacted specimens fail well before buckling occurred. The fact that these specimens do not buckle means that the strain distribution across the specimen width is almost constant at failure. The measured surface strains, membrane surface strains based on an average of the surface strains, and analytical membrane strains are shown in figure 10 for the control specimen just prior to failure. Surface strains are represented by data points and membrane strains are represented by curves. The results show that there is no significant difference in strain across the specimen width so impact location does not affect maximum load-carrying ability.

$[\pm 45/0_2]_s$ specimens.- Two ten-inch-wide specimens were impacted with an impact speed of 150 ft/sec and loaded to failure. Impact locations were at midlength and at the center or one inch from the specimen unloaded edge. Each specimen buckled into one transverse and two axial half-waves then continued to carry the load well into the postbuckling range. The specimens then exhibited a mode shape change to three axial half-waves and failed at a loaded edge. The normalized load versus normalized end-shortening relationship for these two specimens is shown in figure 11. The impact has little effect on the specimen prebuckling behavior, buckling load or postbuckling behavior.

$[\pm 45/0_2]_{3s}$ specimens.- Nine specimens were constructed from graphite-epoxy tape and loaded to failure. Each specimen was 14 inches long and 10 inches wide. Each specimen buckled into one half-wave in each direction prior to failure. Failures occurred at a loaded edge in all cases and caused damage growth at the impact sites for the specimens impacted at high impact speeds. Visible damage was caused by impacts of 300 ft/sec and the impactor passed through the specimen for impacts with speeds greater than 400 ft/sec. Three specimens were impacted at the center, two were impacted two inches from an unloaded edge and two were impacted one inch from an unloaded edge, providing results for impact sites at x/b=.5, .2, and .1, respectively.

The relationship between normalized failure load and impact speed is shown in figure 12. Centrally located impacts and impacts at x/b=.2 do not cause a reduction in maximum load-carrying capability at impact speeds up to 450 ft/sec. However, impacts at speeds above 300 ft/sec at x/b=.1 cause significant reduction in maximum

load-carrying capability. An impact at 450 ft/sec at x/b=.1 can cause a 30 percent reduction in failure load compared to the control specimen.

The experimentally and analytically determined normalized load versus normalized end-shortening relationships for the control specimen are shown in figure 13. The analytical and experimental results for the control specimen agree quite well and each method predicts a normalized buckling load of about 6500 psi. Specimen failure is at 3.1 times the buckling load. The normalized load versus normalized end-shortening behavior of the centrally impacted and both of the side-impacted specimens that were impacted at 450 ft/sec are shown in figure 14. Once again, prebuckling behavior is approximately the same for the three specimens and initial postbuckling behavior is also the same for the three specimens.

The axial strain distribution across the width of a control specimen at midlength is shown in figure 15. The change in analytically determined strain distribution as the load is increased past the buckling load to specimen failure is shown in figure 15(a) and the experimental and analytical membrane strains at failure are shown in figure 15(b). The data points represent surface strains measured by strain gages. The solid and dashed curves represent membrane strains determined from averaging back-to-back surface strain gage results and from finite-element analysis, respectively. Higher strains occur at the specimen edges than in the center, as seen before. However, the section of the specimen which experiences higher strains is smaller than that in the previous case. In $[\pm 45/0_2]_{3s}$ specimens, an impact at width position x/b=.2 is not as far into the region of high strain as an impact at width position x/b=.25 in the $[(\pm 45)_2/\overline{90}]_s$ specimens, so the impact at x/b=.2 in the $[\pm 45/0_2]_{3s}$ specimens causes less reduction in maximum load-carrying capability than the impacts at x/b=.25 in the $[\pm 45/0_2]_{3s}$ case. However, an impact at x/b=.1 in the $[\pm 45/0_2]_{3s}$ specimens is in the region of high axial strain so this impact does significantly affect the maximum load-carrying capability of the specimen. Impact damage location has more effect on maximum load-carrying capability for specimens without 0° plies than for specimens with 0° plies since stacking sequence influences how the load is redistributed after buckling.

CONCLUDING REMARKS

An investigation of the behavior of laminated thin and moderately thick graphite-epoxy and graphite-thermoplastic specimens subjected to impact damage and loaded in compression and tension was conducted. Specimens were impacted with a 0.5-inch-diameter aluminum sphere at impact speeds up to 550 ft/sec (impact energy 30.7 ft-lb) either in the center of the specimen or near an unloaded edge prior to loading.

The results of this investigation indicate that impact location in thin tension-loaded specimens dominated by angle plies influences failure load. In these specimens, impacts near an unsupported edge reduced specimen maximum load-carrying capability more than central impacts (away from an unsupported edge) reduced specimen maximum load-carrying capability. However, the failure load of thin tension-loaded specimens with 50 percent 0° plies was independent of impact location. Experimental results and finite-element analysis results of compression-loaded specimens indicate that high axial strains occur near the simply-supported unloaded edges of a postbuckled specimen. These strains lead to lower failure loads in specimens impacted near the unloaded edge than in specimens impacted away from an edge. The failure load for damaged specimens that fail prior to buckling is unaffected by the widthwise location of the impact damage. Impact damage to

specimens with 0° plies is less dependent upon impact location than impact damage to specimens without 0° plies.

References

1. Starnes, J. H., Jr.; and Williams, J. G.: Failure Characteristics of Graphite-Epoxy Structural Components Loaded in Compression. Mechanics of Composite Materials, Pergamon Press, 1982, pp. 283-306.

2. Jegley, Dawn C.: Compression Behavior of Graphite-Thermoplastic and Graphite-Epoxy Panels with Circular Holes or Impact Damage. NASA TP 3071, March 1991.

3. Guynn, E. G.; and O'Brien, T. K.: The Influence of Lay-Up and Thickness on Composite Impact Damage and Compression Strength. A Collection of Technical Papers--AIAA/ASME/ASCE/AHS 26th Structures, Structural Dynamics and Materials Conference, Part 1, April 1985, pp. 187-196. AIAA Paper No. 85-0646.

4. Starnes, James H., Jr.; and Rouse, Marshall: Post-buckling and Failure Characteristics of Selected Flat Rectangular Graphite-Epoxy Plates Loaded in Compression. A Collection of Technical Papers--AIAA/ASME/ASCE/AHS 22nd Structures, Structural Dynamics and Materials Conference, Part 1, April 1981, pp. 423-434. AIAA Paper No. 81-0543.

5. Avva, V. S.: Fatigue/Impact Studies in Laminated Composites. AFWAL-TR-3060, May 1983.

6. Dorey, Graham: Damage Tolerance and Damage Assessment in Advanced Composites. Advanced Composites, edited by Ivana Partridge, Elsevier Applied Science, 1989, pp. 369-398.

7. Starnes, J. H., Jr.; Rhodes, M. D.; and Williams, J. G.: Effect of Impact Damage and Holes on the Compression Strength of a Graphite/Epoxy Laminate. Nondestructive Evaluation and Flaw Criticality for Composite Materials, edited by R. B. Pipes, ASTM STP 696, 1979, pp. 145-171.

8. Almroth, B.O.; and Brogan, F.A.: The STAGS Computer Code. NASA CR-2950, 1980.

Table I. Stacking Sequence, Average Specimen Dimensions and Control Specimen Normalized Failure Load

Stacking Sequence	Material*	Average Thickness, t (in.)	Average Width, b (in.)	Average Length, L (in.)	Number of Specimens Tested	Normalized Failure Load+, P/A (ksi)
Tension-loaded Specimens						
$[(\pm 45)_2/\overline{90}]_s$	ge,tape	.0498	3.00	10.01	7	32.8
$[\pm 45/0_2]_s$	ge,tape	.0435	3.00	10.00	8	128.
Compression-Loaded Specimens						
$[(\pm 45)_2/\overline{90}]_s$	ge,tape	.0481	3.00	10.00	12	19.7
$[(\pm 45)_2/\overline{90}]_s$	ge,tape	.0479	4.00	10.00	4	15.6
$[(\pm 45)_2/\overline{90}]_s$	gt,tape	.0491	2.99	9.92	14	20.6
$[(\pm 45)_2/\overline{90}]_s$	gt,tape	.0495	4.00	10.00	3	16.4
$[(\pm 45)_2/\overline{90}]_s$	gt,fabric	.0470	3.00	10.00	12	21.2
$[(\pm 45)_2/\overline{90}]_s$	gt,fabric	.0461	4.00	10.00	4	17.8
$[(\pm 45)_2/90]_{3s}$	ge,tape	.1626	3.00	10.00	12	53.0
$[(\pm 45)_2/90]_{3s}$	ge,tape	.1610	4.00	10.00	4	49.4
$[\pm 45/0_2]_s$	ge,tape	.0428	10.00	14.00	3	Not Available
$[\pm 45/0_2]_{3s}$	ge,tape	.1280	10.00	14.00	9	20.4

* ge represents graphite-epoxy, gt represents graphite-thermoplastic, tape represents unidirectional tape and fabric represents woven fabric with ±45 fibers.
+ Normalized failure load of control specimen (failure load/cross-sectional area).

Table II. Relationship Between Impact Speed and Energy

Impact Speed (ft/sec)	Impact Energy (ft-lb)
0.	0.00
50.	0.25
100.	1.02
150.	2.29
200.	4.07
250.	6.35
300.	9.15
350.	12.4
400.	16.3
450.	20.6
500.	25.4
550.	30.7

Table III. Graphite-epoxy Material Properties

Longitudinal Young's modulus, Msi	18.5
Transverse Young's modulus, Msi	1.64
Shear modulus, Msi	.89
Major Poisson's ratio	.30

Table IV. Tension-loaded Specimens

Nominal impact speed, v (ft/sec)	Normalized Failure Load, P/A* (ksi)	
	$x/b^+=.5$	$x/b^+=.2$
stacking sequence $[(\pm45)_2/90]_s$		
200.	27.2	24.6
300.	23.2	16.8
400.	22.6	19.3
stacking sequence $[\pm45/0_2]_s$		
100.	116.	-
200.	103.	105.
300.	98.	91.
400.	105.	116.

* P is the failure load; A is the average cross-sectional area and is .149 in.^{2} for $[(\pm45)_2/90]_s$ specimens, and is .131 in.^{2} for $[\pm45/0_2]_s$ specimens.
+ Panel width (b) is 3 in., x is distance from specimen unloaded edge.

Table V. Compression-loaded Three-inch-wide Specimens

Nominal Impact Speed, v (ft/sec)	Normalized Failure Load, P/A* (ksi)					
stacking sequence $[(\pm45)_2/\overline{90}]_s$						
	graphite-epoxy, tape		graphite-thermoplastic, tape		graphite-thermoplastic, fabric	
	$x/b^+=.5$	$x/b^+=.25$	$x/b^+=.5$	$x/b^+=.25$	$x/b^+=.5$	$x/b^+=.25$
100.	20.2	20.5	21.6	21.9	22.9	23.8
175.	20.7	15.6	21.5	18.4	23.7	22.0
225.	17.8	-	-	-	-	-
250.	18.5	12.9	17.5	16.4	19.1	17.8
300.	18.8	-	12.7	-	-	-
325.	-	15.6	13.6	12.3	17.8	14.8
350.	17.8	-	16.2	-	-	-
375.	-	-	-	-	16.5	-
400.	19.2	-	16.3	-	18.1	13.6
400.	-	-	13.9	-	-	-
500.	-	-	17.6	-	-	-
stacking sequence $[(\pm45)_2/90]_{3s}$						
100.	51.4	50.7	-	-	-	-
175.	27.0	29.0	-	-	-	-
250.	19.6	22.7	-	-	-	-
325.	16.0	-	-	-	-	-
400.	15.2	15.5	-	-	-	-
540.	20.2	17.0	-	-	-	-

* P is the failure load; A is the average cross-sectional area and is .144, .147 and .141 in.^{2}, for the graphite-epoxy, graphite-thermoplastic tape, and graphite-thermoplastic fabric $[(\pm45)_2/\overline{90}]_s$ specimens, respectively. Average cross-sectional area is .488 in.^{2} for the $[(\pm45)_2/90]_{3s}$ specimens.
+ Panel width (b) is 3 inches, x is distance from specimen unloaded edge.

Table VI. Compression-loaded Four-inch-wide Specimens

Material	Nominal impact speed, v (ft/sec)	Normalized Failure Load, P/A* (ksi)		
	stacking sequence $[(\pm 45)_2/\overline{90}]_s$			
		$x/b^+=.5$	$x/b^+=.3$	$x/b^+=.2$
graphite-epoxy, tape	450.	15.9	17.0	8.7
graphite-thermoplastic, tape	450.	18.2	-	9.5
graphite-thermoplastic, fabric	450.	18.1	13.8	12.2
	stacking sequence $[(\pm 45)_2/90]_{3s}$			
graphite-epoxy, tape	500.	21.0	18.3	15.5

* P is the failure load; A is the average cross-sectional area and is .192, .198, and .184 $in.^2$, for the graphite-epoxy, graphite-thermoplastic tape, and graphite-thermoplastic fabric $[(\pm 45)_2/\overline{90}]_s$ specimens, respectively. Average cross-sectional area is .644 $in.^2$ for the $[(\pm 45)_2/90]_{3s}$ specimens.
+ Panel width (b) is 4 inches, x is distance from specimen unloaded edge.

Table VII. Compression-loaded Ten-inch-wide Specimens

Nominal impact speed, v (ft/sec)	Normalized Failure Load*, P/A (ksi)		
stacking sequence $[\pm 45/0_2]_{3s}$			
	$x/b^+=.5$	$x/b^+=.2$	$x/b^+=.1$
250.	23.4	21.8	-
350.	21.0	21.6	16.2
450.	20.9	21.2	14.3
stacking sequence $[\pm 45/0_2]_s$			
150.	9.98	-	9.1

* P is the failure load; A is the average cross-sectional area and is .428 $in.^2$ for $[\pm 45/0_2]_s$ specimens, and 1.28 $in.^2$ for $[\pm 45/0_2]_{3s}$ specimens.
+ Panel width (b) is 10 in., x is distance from specimen unloaded edge.

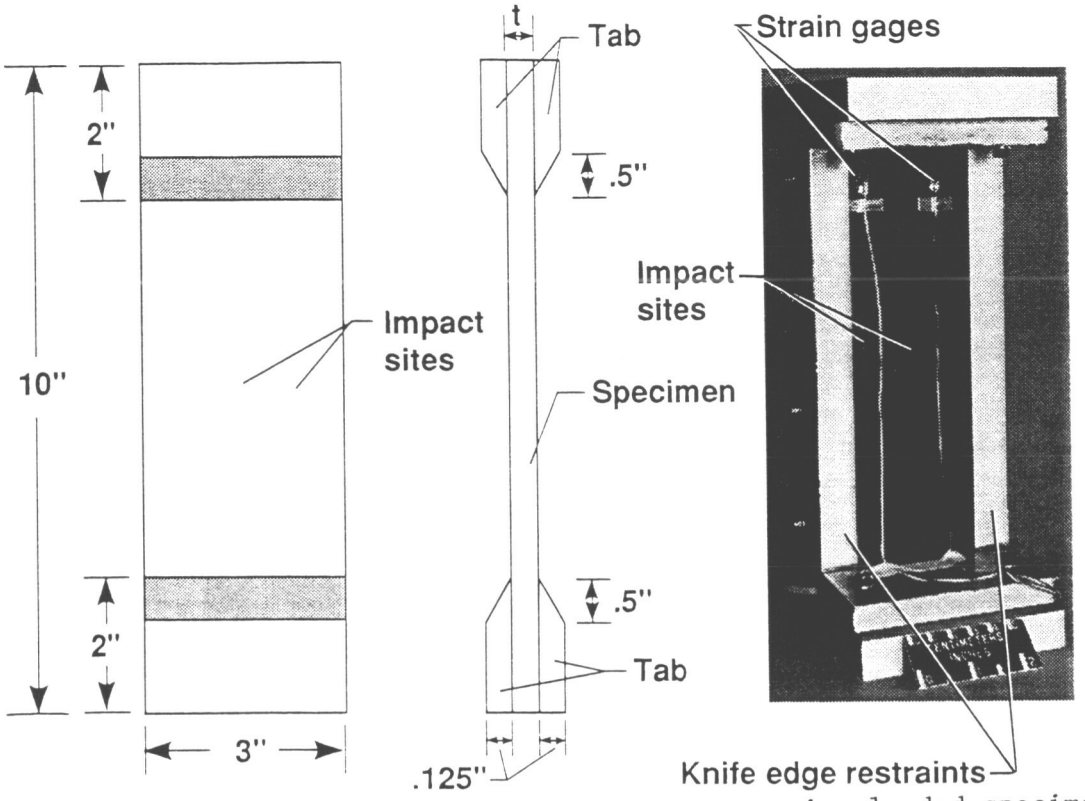

1 (a) Tension-loaded specimens. 1 (b) Compression-loaded specimens.

Figure 1. Specimen configuration.

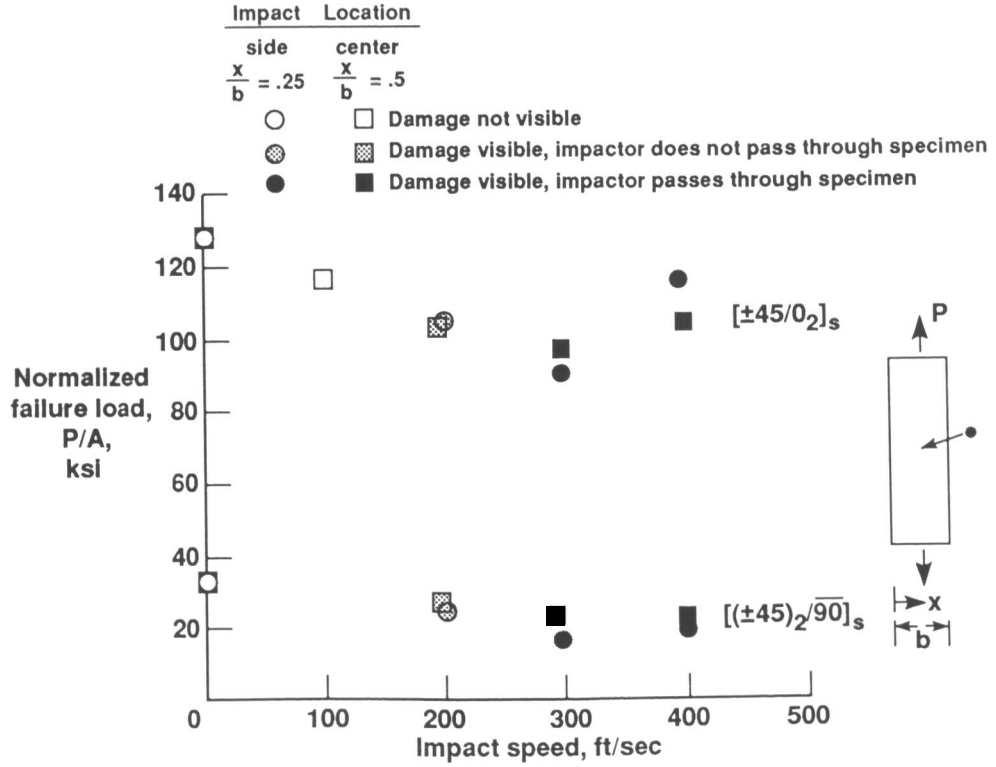

Figure 2. Effect of impact speed on normalized tensile failure load for panels with stacking sequences $[(\pm 45)_2/\overline{90}]_s$ and $[\pm 45/0_2]_s$ impacted in the center and at the side. A is cross-sectional area.

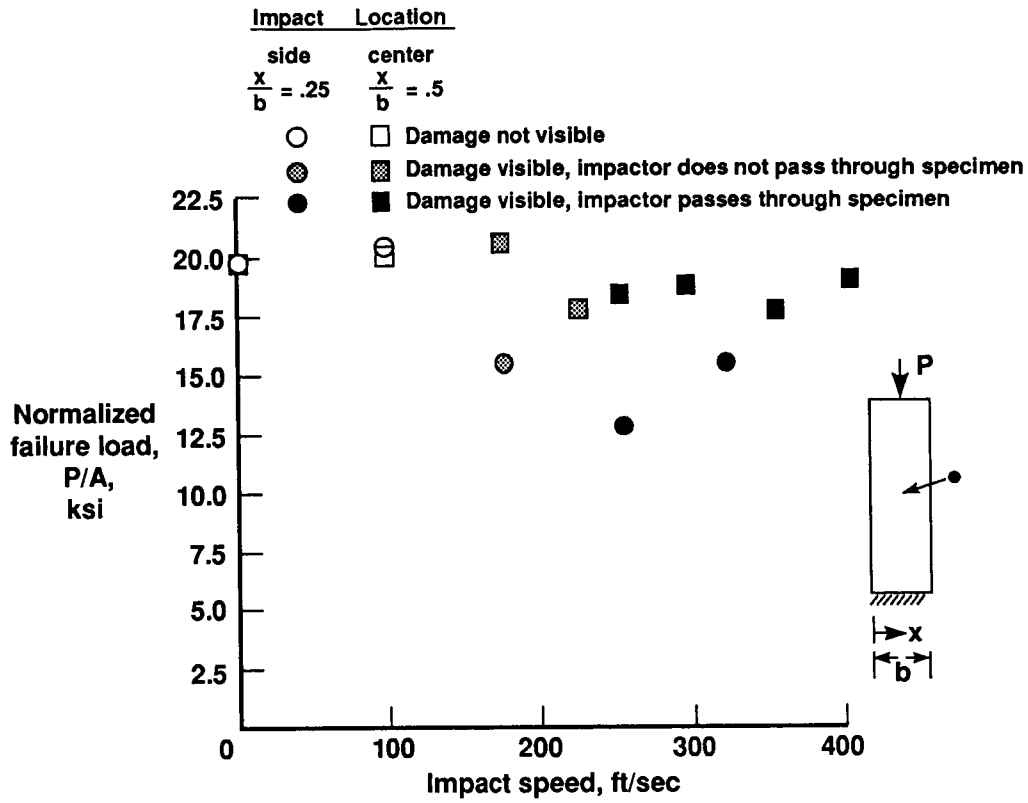

3 (a) Graphite-epoxy tape specimens.

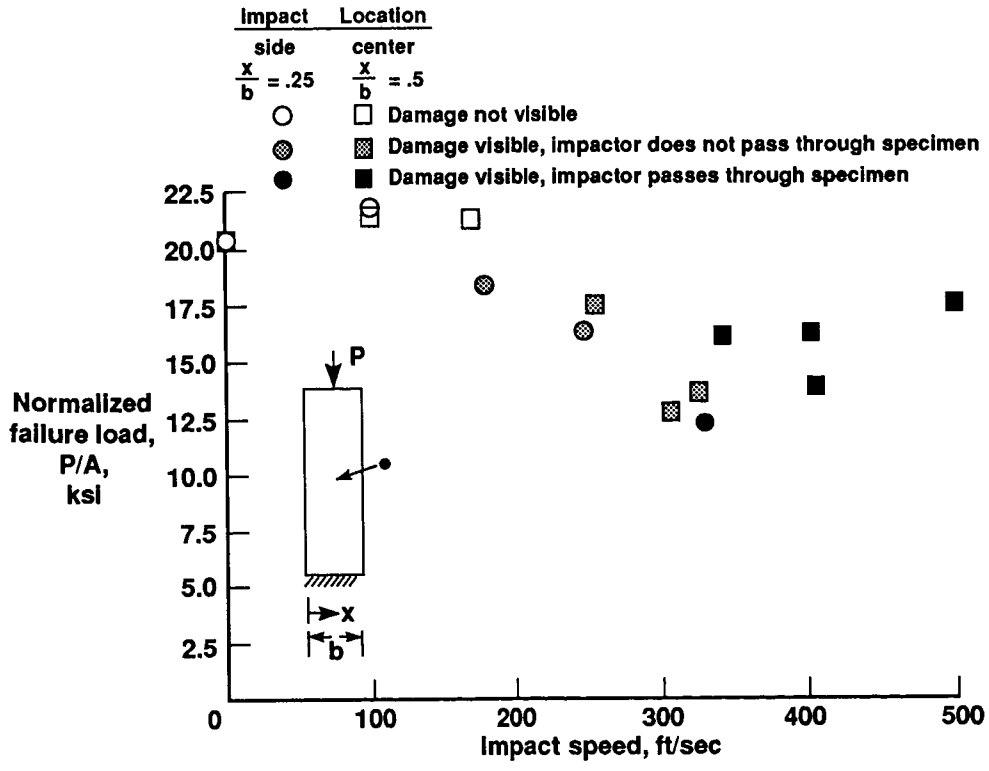

3 (b) Graphite-thermoplastic tape specimens.

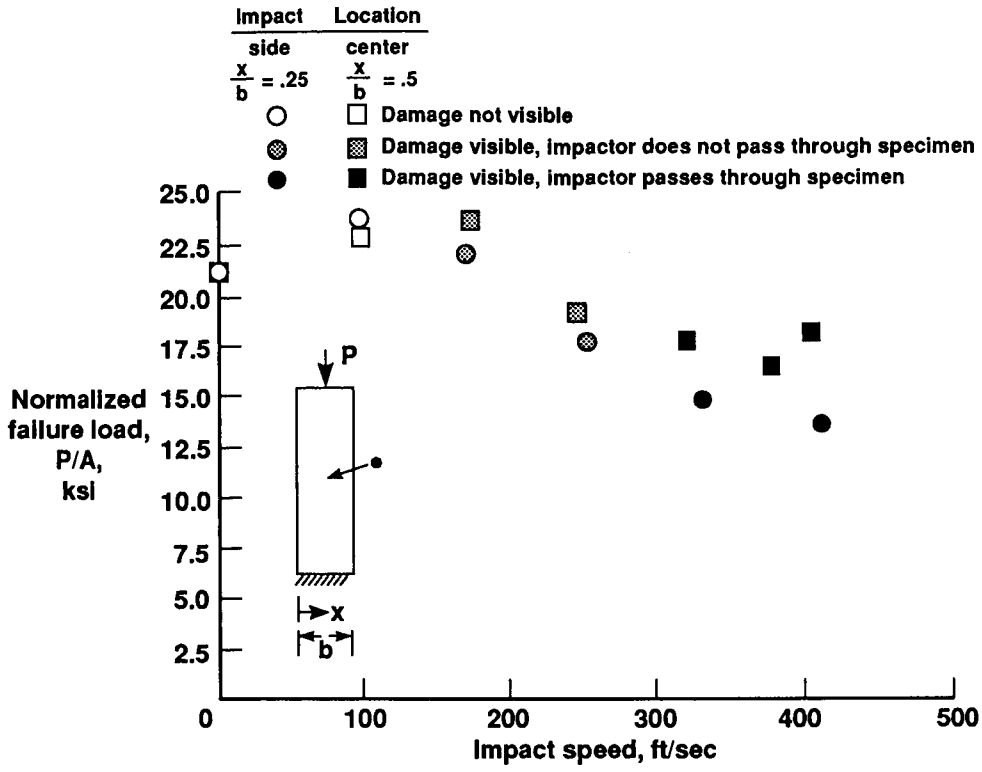

3 (c) Graphite-thermoplastic fabric specimens.

Figure 3. Effect of impact speed on compressive failure load for panels with a $[(\pm 45)_2/\overline{90}]_s$ stacking sequence impacted in the center and at the side. A is cross-sectional area.

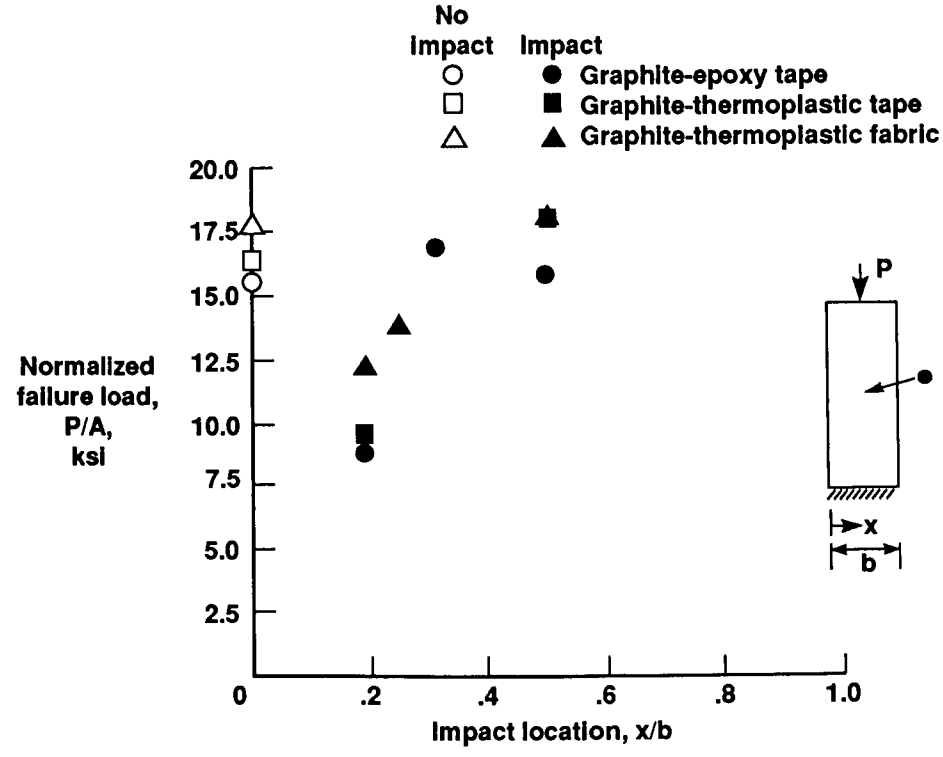

Figure 4. Normalized compressive failure load as a function of impact location for panels with a $[(\pm 45)_2/\overline{90}]_s$ stacking sequence impacted at 450 ft/sec. A is cross-sectional area.

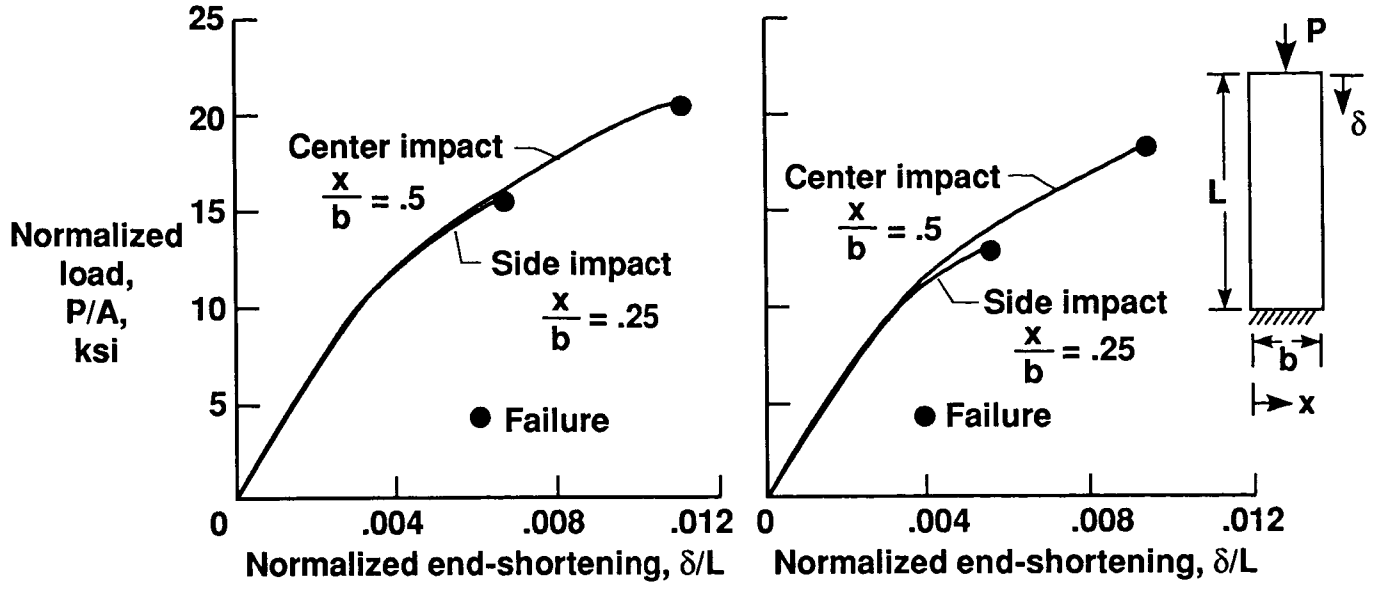

5 (a) Impact damage barely visible prior to load (impact speed 175 ft/sec).

5 (b) Severe impact damage (impact speed 250 ft/sec).

Figure 5. Normalized load versus normalized end-shortening for graphite-epoxy panels with a $[(\pm 45)_2/\overline{90}]_s$ stacking sequence impacted at the center or side with the same impact speed. A is cross-sectional area.

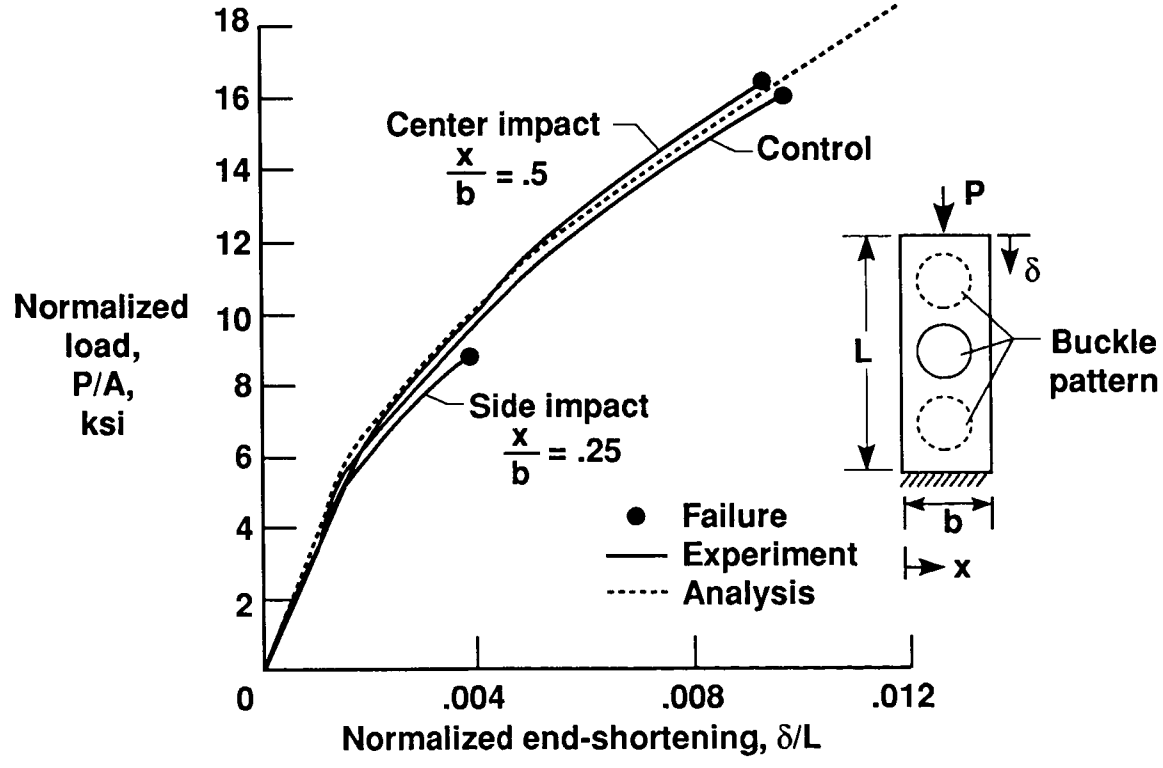

6 (a) Normalized load versus normalized end-shortening. A is cross-sectional area.

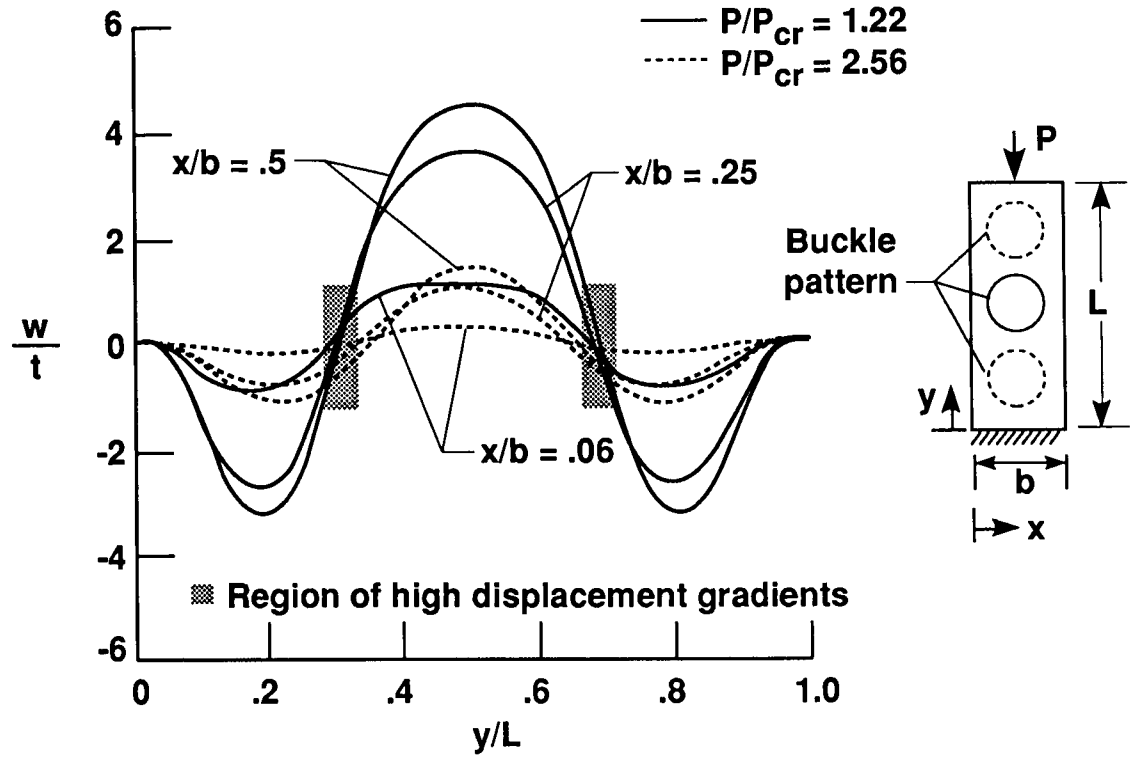

6 (b) Normalized out-of-plane displacement versus axial location at two values of load.

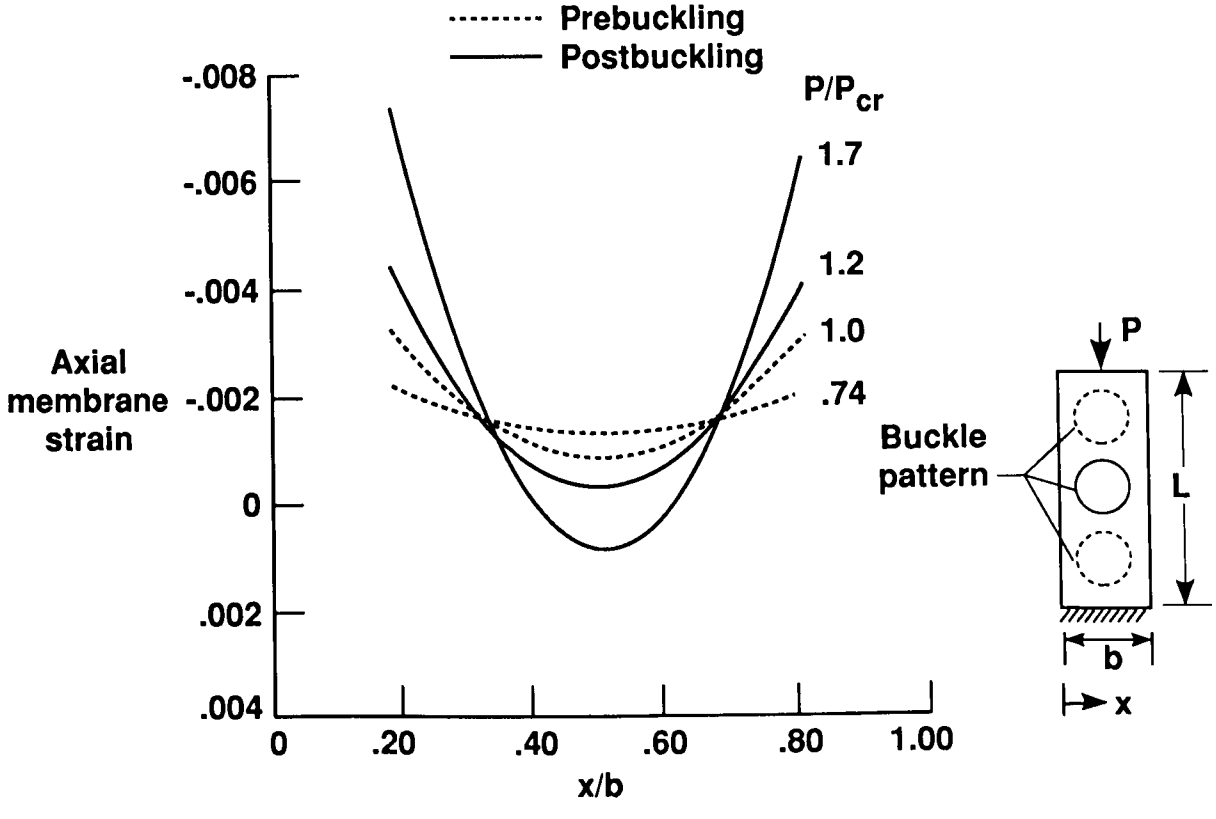

6 (c) Axial membrane strain versus normalized width location for various load levels at a nodal line.

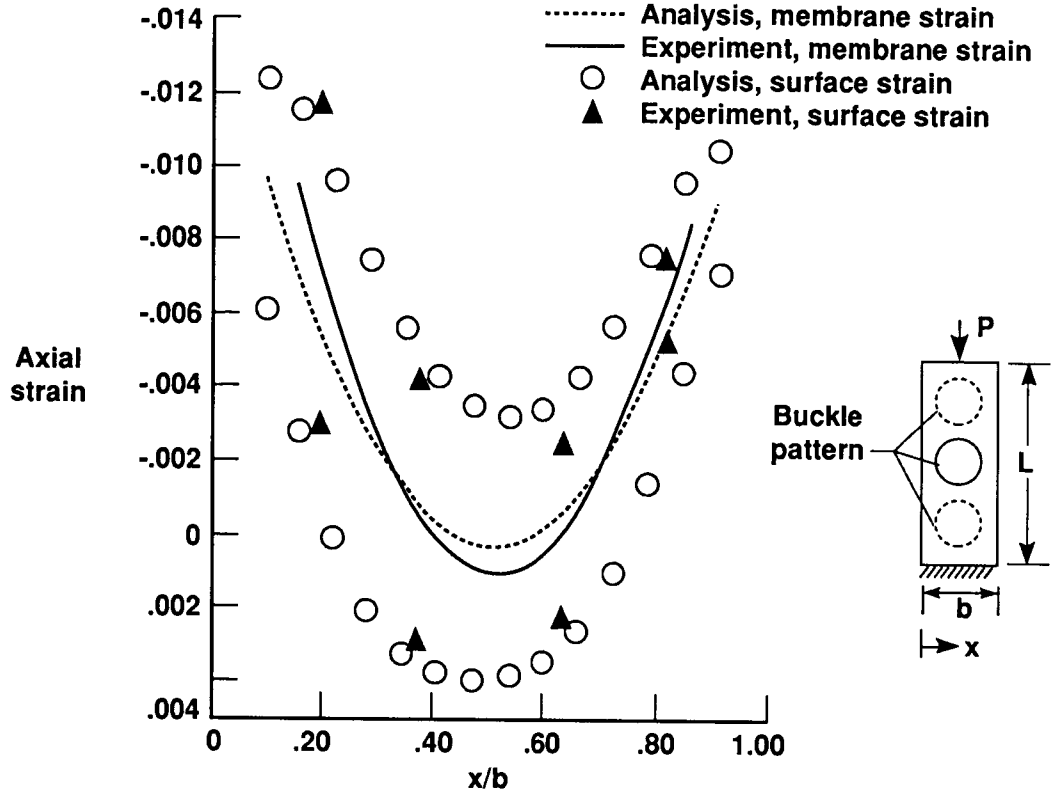

6 (d) Strain versus width location at failure.

Figure 6. Analytically determined displacements and strains for four-inch wide control panels with a $[(\pm 45)_2/\overline{90}]_s$ stacking sequence.

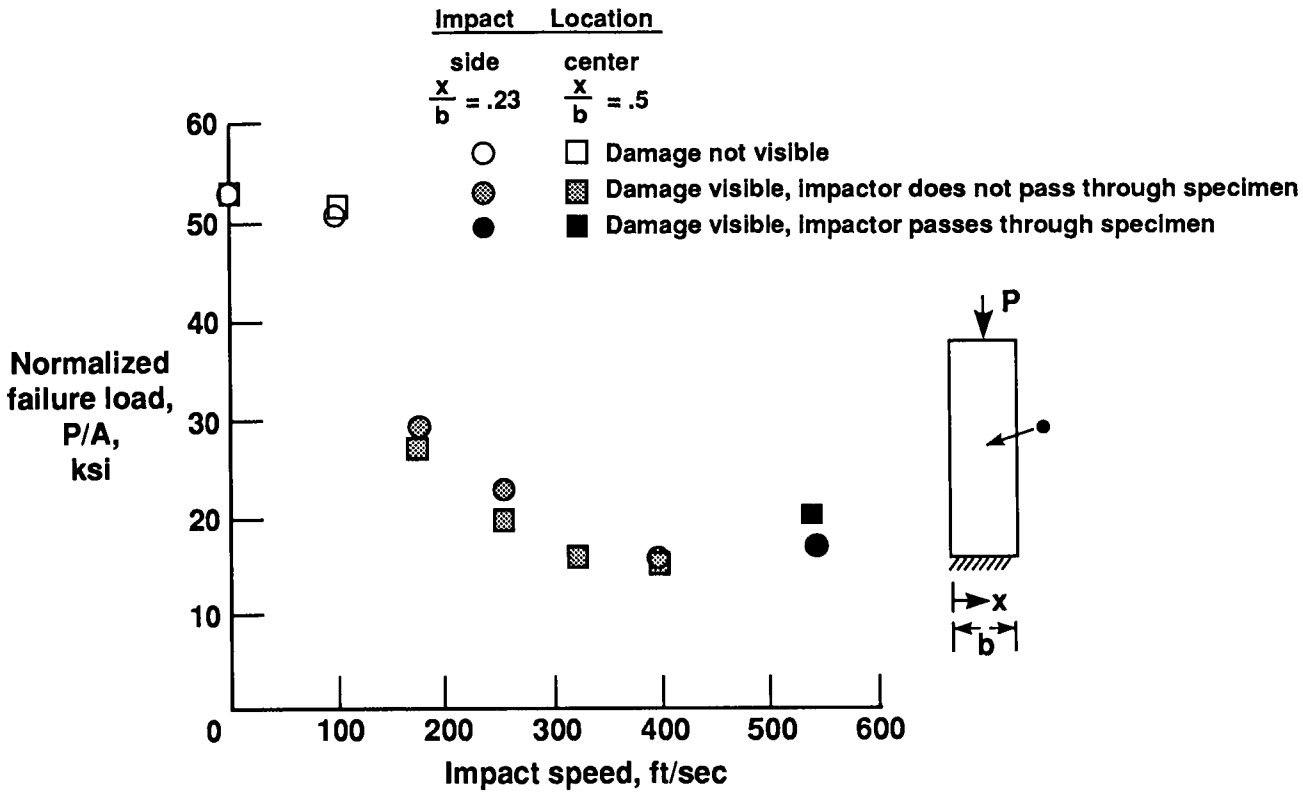

Figure 7. Effect of impact speed on normalized compressive failure load for panels with a $[(\pm 45)_2/90]_{3s}$ stacking sequence impacted in the center and at the side. A is cross-sectional area.

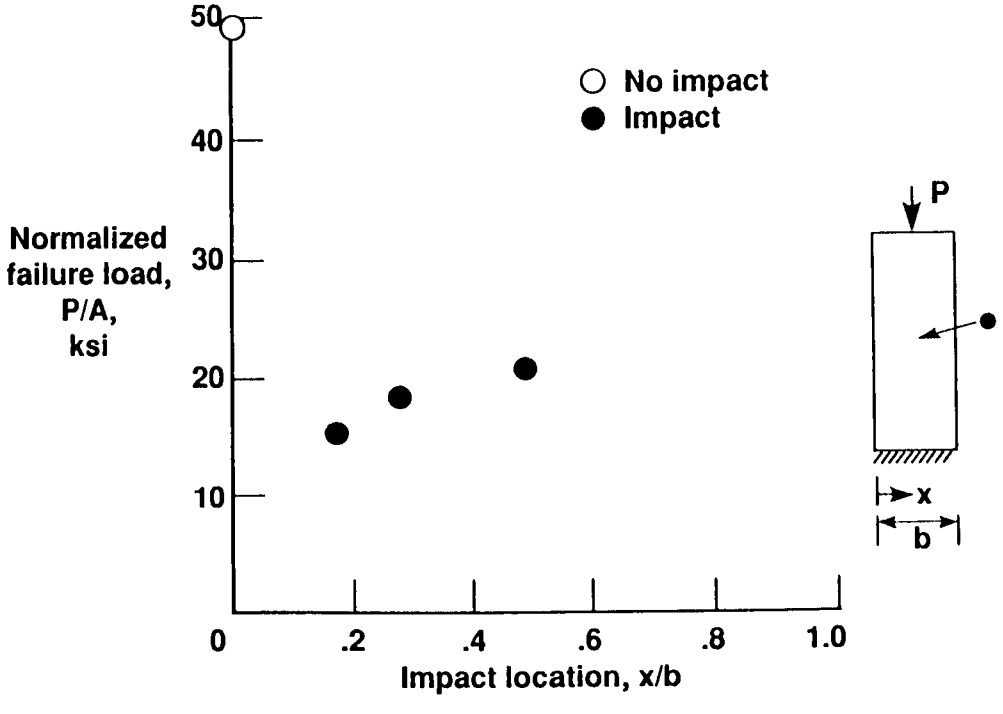

Figure 8. Normalized compressive failure load as a function of impact location four-inch wide panels with a $[(\pm 45)_2/90]_{3s}$ stacking sequence impacted at 500 ft/sec. A is cross-sectional area.

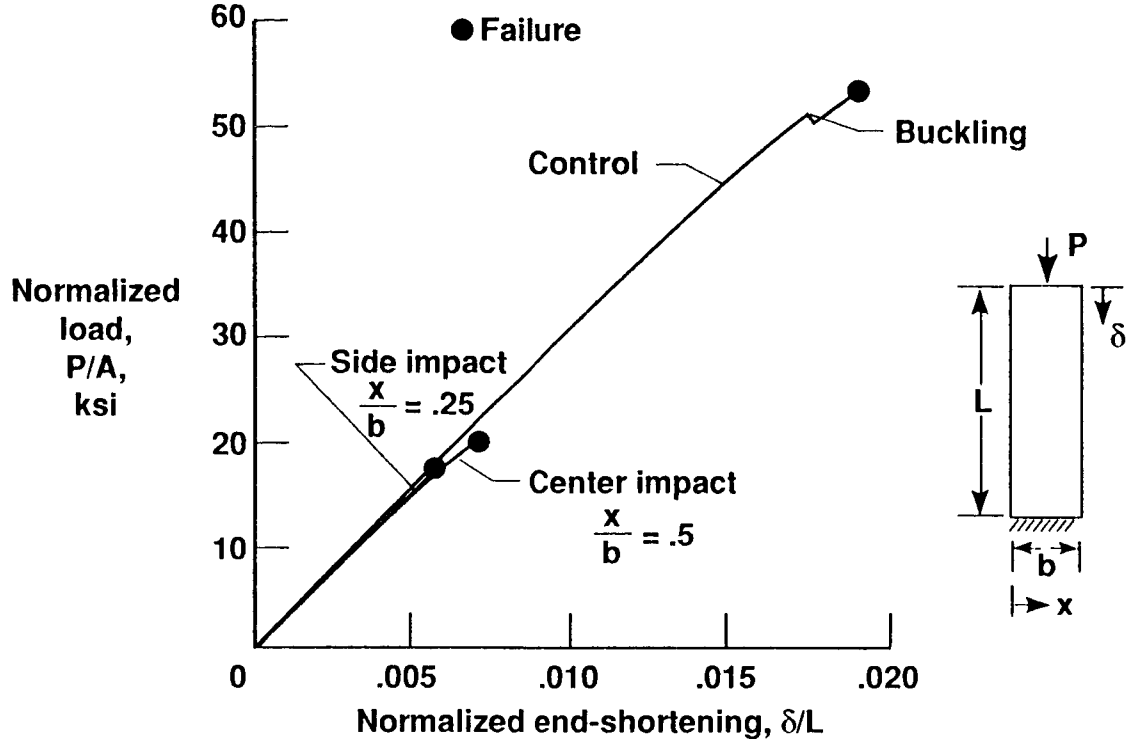

Figure 9. Normalized load versus normalized end-shortening for graphite-epoxy panels with a $[(\pm 45)_2/90]_{3s}$ stacking sequence with no impact and impacted at the center or side at 540 ft/sec. A is cross-sectional area.

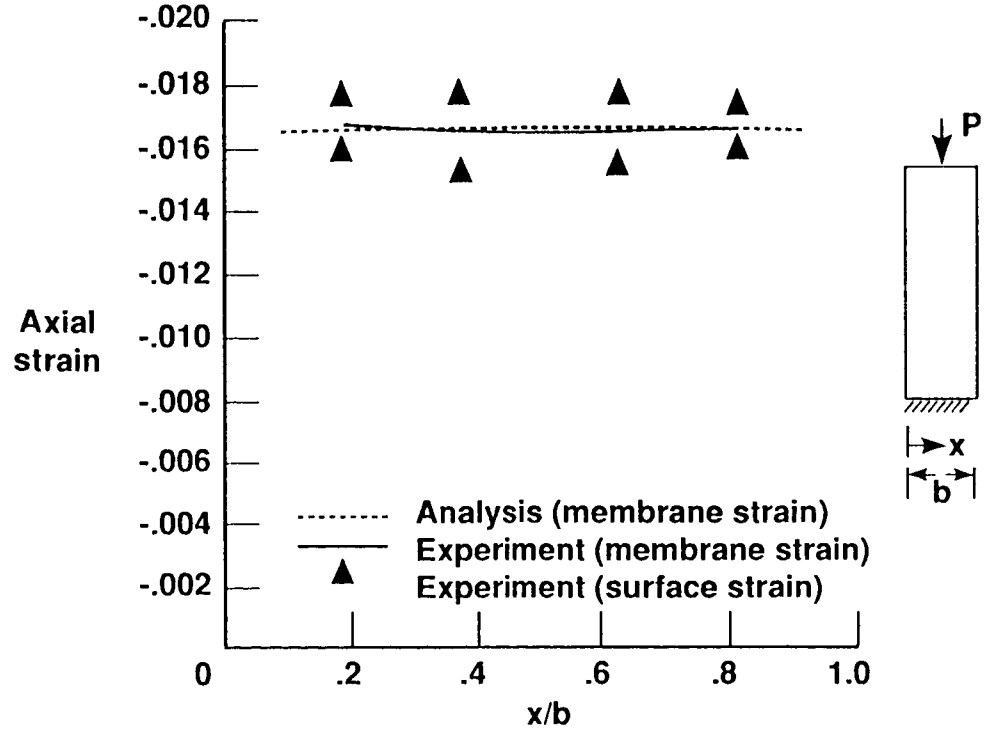

Figure 10. Strain versus normalized width location at failure of four-inch wide control panel with a $[(\pm 45)_2/90]_{3s}$ stacking sequence.

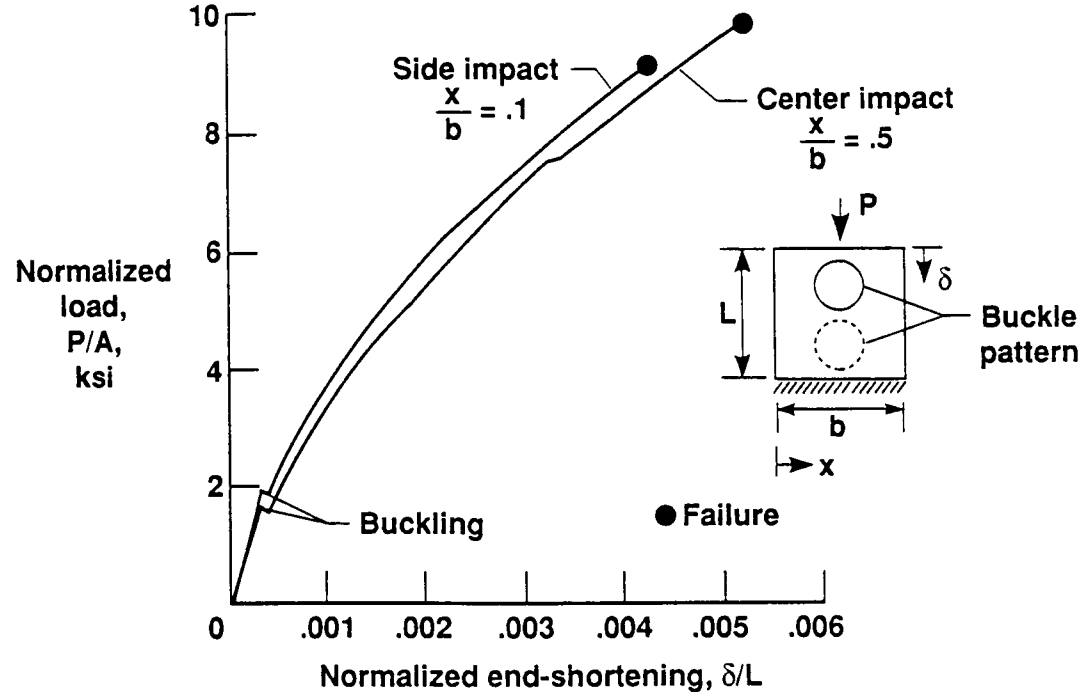

Figure 11. Normalized load versus normalized end-shortening for graphite-epoxy panels with a $[\pm 45/0_2]_s$ stacking sequence impacted at the center or side with an impact speed of 150 ft/sec, causing barely visible damage prior to load. A is cross-sectional area.

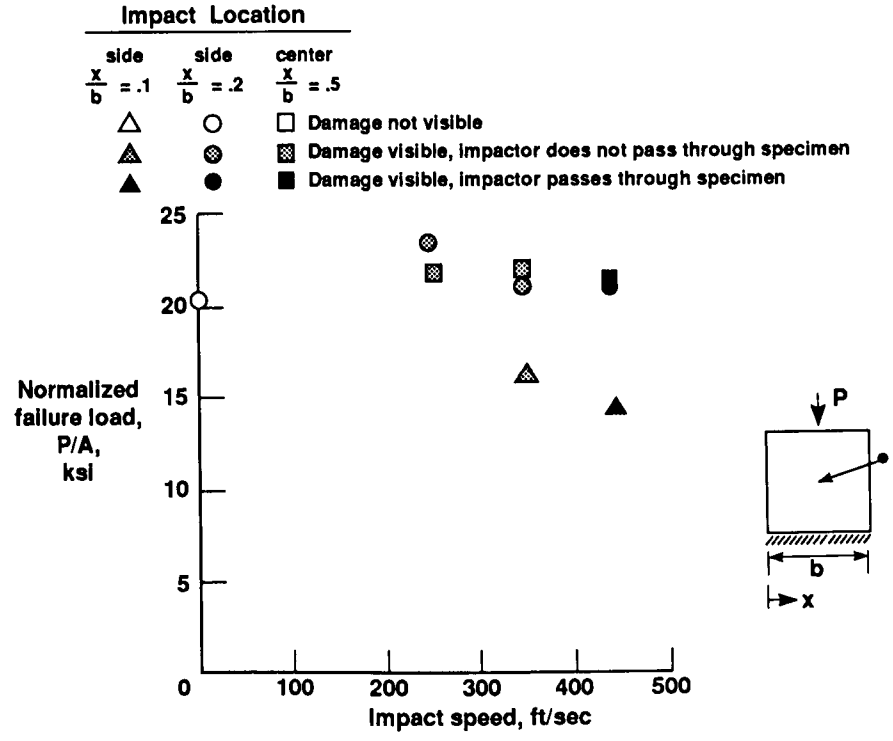

Figure 12. Effect of impact speed on normalized compressive failure load of graphite-epoxy panels with a $[\pm 45/0_2]_{3s}$ stacking sequence. A is cross-sectional area.

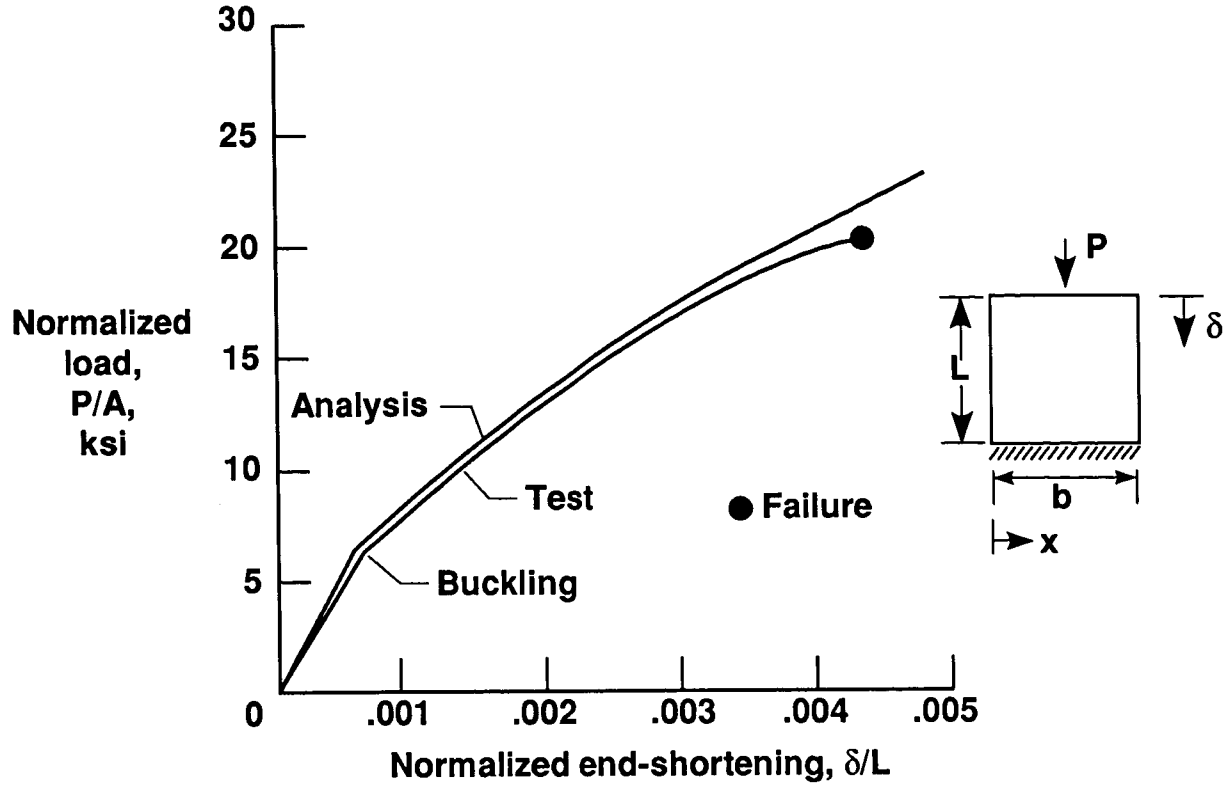

Figure 13. Normalized load versus end-shortening for control panel with a $[\pm 45/0_2]_{3s}$ stacking sequence. A is cross-sectional area.

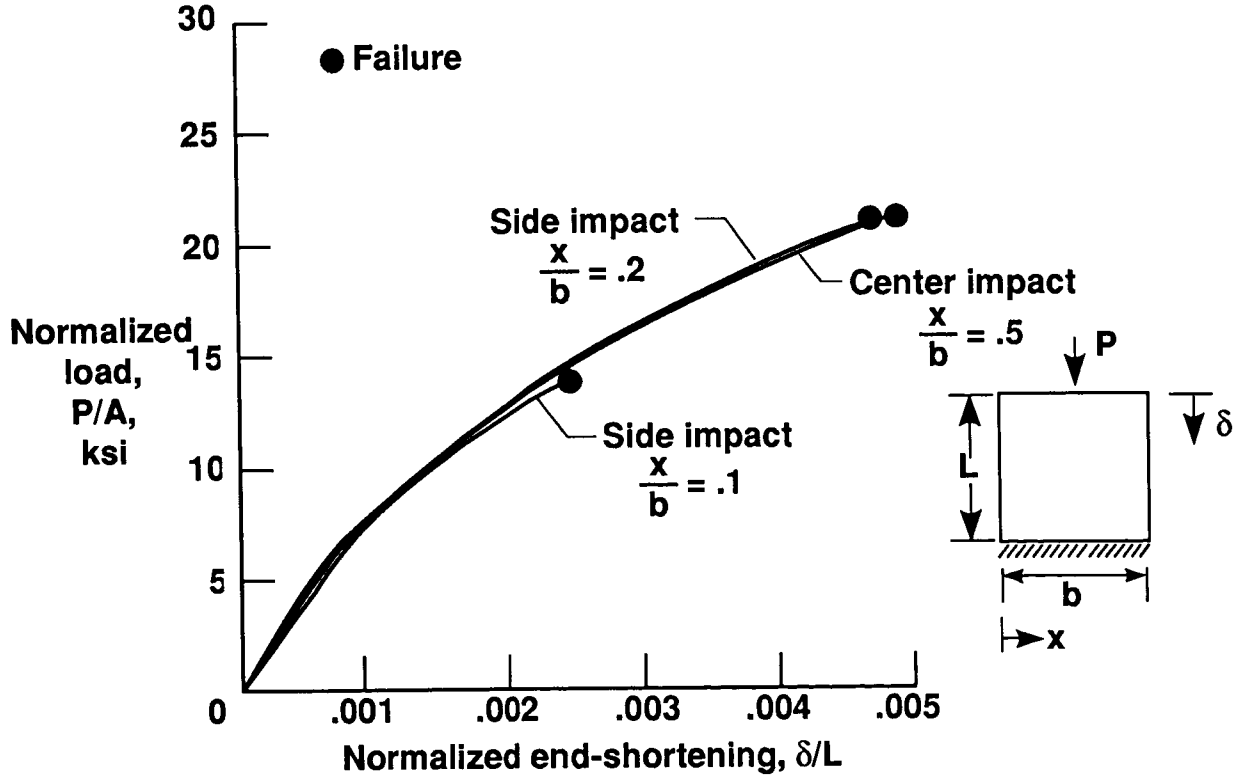

Figure 14. Normalized load versus normalized end-shortening for panels with a $[\pm 45/0_2]_{3s}$ stacking sequence impacted at 450 ft/sec in the center and at two side locations. A is cross-sectional area.

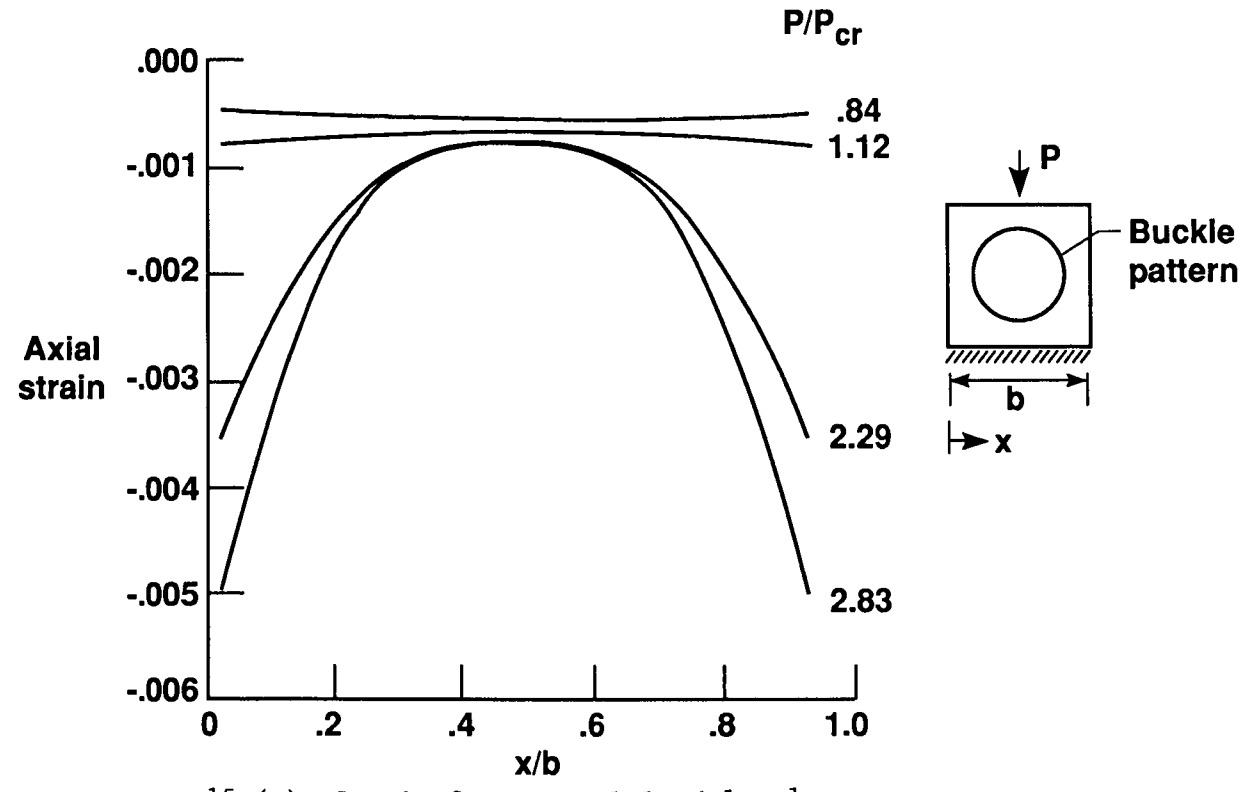

15 (a) Strain for several load levels.

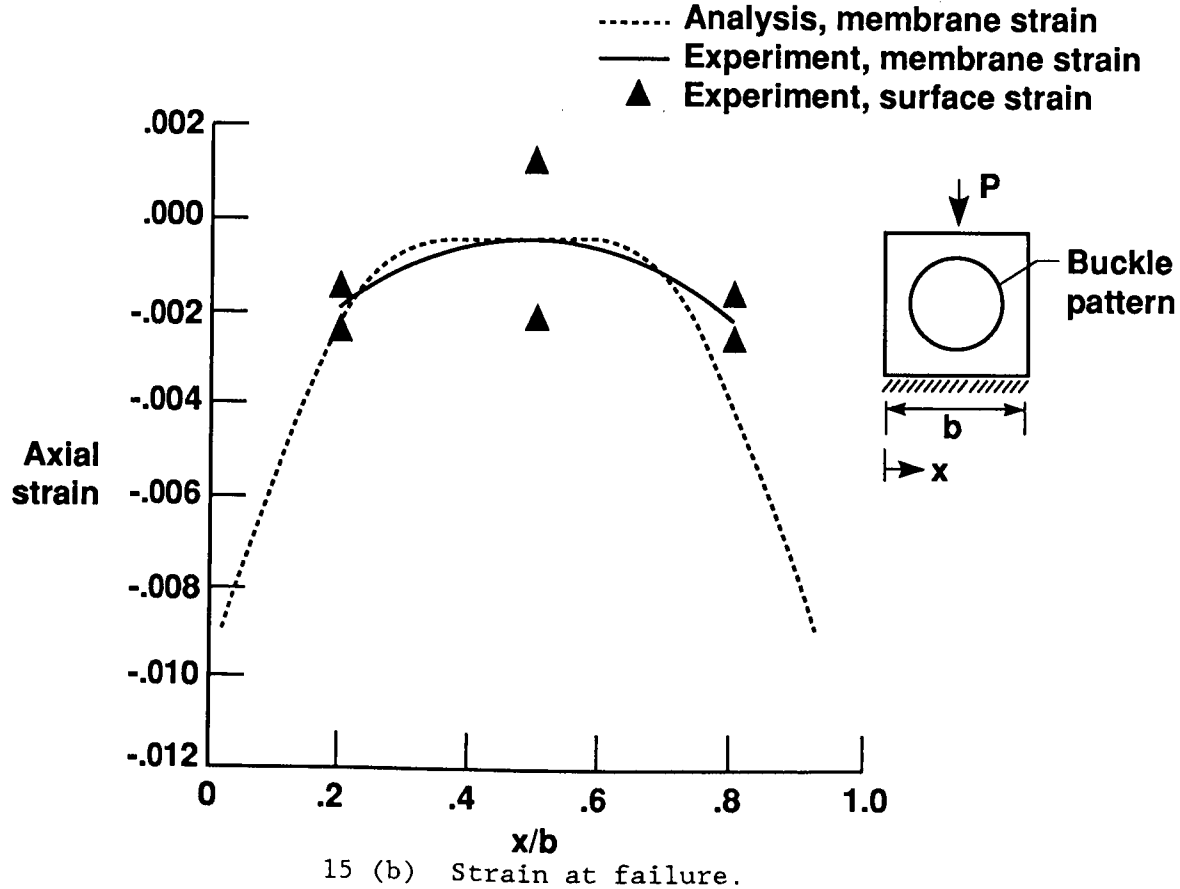

15 (b) Strain at failure.

Figure 15. Strain versus width location of ten-inch wide control panel at axial centerline with a $[\pm 45/0_2]_{3s}$ stacking sequence.